Asynchronous changes of CO_2, H_2 and He concentrations in soil gases: a theoretical model and experimental results

Roberto M. R. Di Martino[1], Marco Camarda[1], Sergio Gurrieri[1], Mariano Valenza[2]

[1]Istituto Nazionale di Geofisica e Vulcanologia, sezione di Palermo – via Ugo La Malfa, 153 – 90146 Palermo, Italy

Correspondence to: robertomr.dimartino@gmail.com

[2]Dipartimento DiSTeM, Università di Palermo, via Archirafi 36, 90123 Palermo, Italy

This article has been accepted for publication and undergone full peer review but has not been through the copyediting, typesetting, pagination and proofreading process which may lead to differences between this version and the Version of Record. Please cite this article as doi: 10.1002/2015JB012600

Abstract

This paper focuses on the chemical composition changes in soil gases through both a theoretical model and laboratory experiments. The model describes the one-dimensional mass transfer process, which is triggered by changes in the flux parameters of the system, and the time-dependent evolution of the composition of the soil gases as a function of i) the pristine gas mixture, ii) the diffusivity of the chemicals, and iii) the thickness of the transited medium. Carbon dioxide (CO_2), hydrogen (H_2), and helium (He) were used in a laboratory-scale flux simulator to investigate the evolution of the gas composition profile in an artificial soil of constant thickness. The agreement between the theoretical calculations and the experimental results supports the validity of the model. Our results indicate a good reproducibility of the transient changes in the concentrations of CO_2, He, and H_2 in CO_2-rich gas mixtures that contain He and H_2 as trace gases. Finally, the theoretical results were used to analyze the H_2 and CO_2 continuous monitoring data collected at Etna volcano in 2010.

Key points

- Asynchronous changes in volcanic gas composition are related with the depth of the gas source.
- The advective-diffusive transport processes accounts for the separation of the soil gas components.
- H_2 and CO_2 emissions at Mt Etna show a connection with the source of the volcanic tremor.

Index terms: 8430, 8419, 8410, 0330, 1009.

Key words: Soil gases, Volcanic gas composition, Volcano monitoring, Hydrogen, Carbon dioxide, Helium.

1. Introduction

A thorough understanding of gas transport dynamics in soils is of considerable interest in many fields of science and engineering. The potential applications of this knowledge include environmental issues associated with contaminant transport [*Jury et al.,* 1983; *Taylor et al.,* 1990; *Sleep,* 1998; *Yates et al.,* 2000; *Berkowitz,* 2002; *Ptak et al.,* 2004; *Köhne et al.,* 2009], agricultural concerns in moisture or nutrient transport, soil-washing practices in chemical industries, and subsurface storing of nuclear waste.

In volcanology, the chemical and isotopic compositions of the gases emitted from both soils and fumaroles are proxies for magmatic activity [*Capasso et al.,* 1992; *Giammanco et al.,* 1995; *Giammanco et al.,* 1998; *Granieri et al.,* 2009*; Camarda et al.,* 2012]. This geochemical approach involves the direct sampling of the volcanic gases [*Giggenbach,* 1987] and subsequent quantitative analysis in the laboratory to investigate the chemical equilibriums. These activities are performed worldwide at many volcano observatories through periodic and in frequent field campaigns. Unfortunately, these campaigns are expensive, time consuming, risky during volcanic unrest, and restricted during eruptive periods.

The investigation of volcanic activity involves the measurement of the chemical composition of gases via spectrometers and electrochemical sensors deployed in the field [*Shinohara,* 2005; *Aiuppa et al.,* 2005; *Shinohara et al.,* 2008; *Aiuppa et al.,* 2008; *Aiuppa et al.,* 2009; *Aiuppa et al.,* 2010a; *Roberts et al.,* 2012; *Di Martino et al.,* 2013; *De Gregorio et al.,* 2013]. In certain localities, many automated devices have been designed and installed as a network to measure the amounts of certain gas components and gas fluxes multiple times per day [*Gurrieri et al.,* 2008]. The datasets obtained from geochemical monitoring networks allow the investigation of the magma dynamics and the evaluation of the gas budget emitted from volcanoes. Recently, this approach has shed light on changes associated with a high rate of

volcanic degassing activity. For instance, the continuous monitoring of H_2 and CO_2 in the ground gases emitted at Mt. Etna indicated that changes in the concentration of H_2 preceded the changes in CO_2 [*Di Martino et al.*, 2013].

According to the concepts discussed above, the chemistry of volcanic gases and the processes occurring in the deep reservoirs are important topics that motivate us to thoroughly investigate the evolution of the gas composition during transport through the rocks. Although the various sources and sink of the different components of the ground gases (e.g., magmatic, biogenic, and fluid-rock exchange sources) and the transport processes through porous materials have been carefully studied [*Carslaw et al.*, 1959; *Isachenko et al.*, 1980; *Hardee*, 1982; *Sahimi*, 1995; *Chiodini et al.*, 1998; *Werner et al.*, 2000; *Gerlach et al.*, 2001; *Chiodini et al.*, 2005; *Camarda et al.*, 2006; *Ho and Webb*, 2006, and references therein], the relationship between the evolution of the chemistry of the gases released in volcanic areas and the depth of the gas source is still poorly understood.

In this paper, we report the development of a simplified analytical solution to describe the compositional changes in gases passing through soils, which are regarded as porous media. In the theoretical framework, a homogeneous porous medium separates the gas reservoir from the Earth's surface. The model includes the effects of both diffusive and advective transport processes resulting from a non-zero concentration gradient and a non-zero pressure gradient, respectively. The approximate analytical approach of the integral method [*Cheng and Cheng*, 2005; *Klaseboer et al.*, 2012] provides a mathematical solution to the fluid flux problem.

Moreover, a gas flux experiment has been designed to check the reliability of the theoretical computations with respect to a laboratory-scale gas flux simulator. In this experiment, the flux tests were performed with pure CO_2, He, and several laboratory gas standards, which were composed of the gas components emitted in volcanic and geothermal areas (i.e., CO_2, He, H_2, O_2, N_2, CH_4, and CO).

2. Modeling

2.1. The advective-diffusive transport process

In this study, we examine the one-dimensional (z axis) gas transport through a homogeneous soil of constant thickness. The upper surface of the soil represents the boundary between the Earth and the atmosphere, and the lower surface represents the boundary of the gas reservoir. The reservoir triggers the perturbation of the gas flux, which induces changes in the compositional profile of the ground gases.

Both diffusive and advective transport processes govern the gas transport through the porous media. The diffusive component of the gas transport is described as follows:

$$\phi_{d(i)} = -D\frac{dC_i}{dz} \tag{1}$$

where $\varphi_{d(i)}$ is the diffusive flux, dC_i/dz is the concentration gradient along the z axis, and D is the bulk diffusivity (or effective diffusion coefficient) of the i^{th} component. According to equation (1), the rate of mass transport per unit cross-sectional area is proportional to the steepness of the concentration gradient, and the transport direction is normal to the diffusion surface. The bulk diffusivity is a substance-dependent quantity and changes as function of the soil properties. As a porous medium, the soil consists of a number of voids and a solid skeleton. This arrangement forms a barrier to the diffusion and reduces the free space for gas leakage. Furthermore, diffusion occurs through the cramped pores of the medium and over a longer distance than that of a straight line because the path through the pores is convoluted. These effects are lumped together in the bulk diffusivity:

$$D = \frac{D_i \cdot p}{\tau} \tag{2}$$

where D_i is the molecular diffusivity of the i^{th} component, p is the void fraction, and τ is the tortuosity of the soil. Tortuosity accounts for the longer distances that the gases must travel through the pores and ranges between two and six, with an average of approximately three

[*Epstein*, 1989; *Sahimi et al.*, 1990].

Both mass and heat transfer process largely occur by advection [*Hardee*, 1982; *Aubert*, 1999]. The dominant component of gas transport through the soils is the advective flux, which is also referred to as the effusive, convective or viscous flux [*Carslaw et al.*, 1959; *Isachenko et al.*, 1980; *Sahimi*, 1995; *Chiodini et al.*, 1998; *Werner et al.*, 2000; Chiodini et al., 2001; *Gerlach et al.*, 2001; *Chiodini et al.*, 2005; *Camarda et al.*, 2006]. The advective component of the mass transfer is expressed as follows:

$$\varphi_a = \nu_{a(i)} \cdot C_i \tag{3}$$

where φ_a is the advective flux, $\nu_{a(i)}$ is the advective flux rate, and C_i is the concentration of the i^{th} component. According to the Darcy's law, the advective velocity is described by equation (4):

$$\nu_{a(i)} = -\frac{k}{\mu} \cdot \frac{dP}{dz} \tag{4}$$

where μ is the dynamic gas viscosity, k is the permeability of the medium, and dP/dz is the pressure gradient along the z axis. The advective component of the mass transfer is proportional to the steepness of the pressure gradient and has the opposite direction of the pressure gradient.

Under a wide range of environmental conditions, the interactions of both advection and diffusion lead to mass transport. Therefore, the most general equation

$$J_i = \varphi_{d(i)} + \varphi_{a(i)} = -D\frac{dC_i}{dz} + C_i \nu_{a(i)} \tag{5}$$

describes the gas flux through the soils [*Camarda et al.*, 2007].

2.2. Algebraic formulation and theoretical results

The one-dimensional model proposed in this paper integrates the advective-diffusive process

with the equation of continuity (Eq. 6):

$$\frac{d}{dz}\left(-D\frac{dC}{dz}+\nu C\right)=\frac{dC}{dt} \tag{6}$$

where dC/dt is the first derivative of the concentration with respect to the time, t. Equation (6) demonstrates that a spatial change in the gas flux produces mass changes in the time domain. To find the solution of equation (6), we assume that the concentration at time t=0 is equal to $C_{initial}$ at any z level in the medium:

$$C = C_{initial} \text{ for } t = 0 \text{ at } z \geq 0. \tag{7}$$

It is worth nothing that assumption made by equation (7) implies the concentration of the i^{th} species is constant in the porous medium, but it can be initially different from zero.

Furthermore, we assume the following boundary condition:

$$C = C_1 \text{ for } t > 0 \text{ at } z = 0 \tag{8}$$

where $C_1$is the forced concentration from the gas reservoir.

Calculation of the definite integral of equation (6), with respect to the space variable in the range z = 0 and $z = \delta_t$, provides the solution of the flux problem:

$$\int_0^{\delta_t}\frac{d}{dz}\left(-D\frac{dC}{dz}+\nu C\right)dz=-\int_0^{\delta_t}\frac{dC}{dt}dz\,. \tag{9}$$

Equation (9) is integrated over a distance δ_t, referred to as the compositional layer (Figure 1). Above the compositional layer, the profile is unaffected by changes in the concentration of the i^{th} component because no mass flux occurs across δ_t.

Solution of equation (9) provides the concentration profile for $z \geq 0$ of the i^{th} gas component in the soil gases, which is initially at a uniform concentration $C_{initial}$. According to Leibniz's rule, equation (9) becomes

$$-D\frac{dC}{dz}+\nu C\Big|_{\delta}-\left(-D\frac{dC}{dz}+\nu C\right)\Big|_0=-\frac{d}{dt}\left(\int_0^{\delta}C\,dz-C\Big|_{\delta}\,\delta\right) \tag{10}$$

where $C|_{\delta}$ represents the concentration of the i^{th} gas component at the distance δ_t (Figure 1).

Additionally,

$$-D\frac{dC}{dz}+\nu C=J \qquad \text{at} \qquad z=0 \tag{11}$$

in the absence of gas sources or sinks in the soil.

According to the strict definition of the compositional layer, at the distance $z = \delta_t$

$$\frac{dC}{dz}=0 \tag{12}$$

and

$$C = C_{initial} \tag{13}$$

The boundary conditions [11], [12], and [13] allow equation (10) to be simplified to

$$\nu C_i - J = -\frac{d}{dt}\left(\int_0^{\delta} C\,dz - C\big|_{\delta}\,\delta\right) \tag{14}$$

The solution of equation (14) is obtained through the approximate approach of the integral method [*Cheng and Cheng,* 2005; *Klaseboer et al.,* 2012] that provides an algebraic solution to the flux problem. The integral method is used in a wide range of engineering problems, such as melting and solidification problems, heat and momentum transfer problems for specified boundary conditions, and transient fluid fluxes through a porous medium with pressure-dependent permeability [*Wu and Pruess,* 2000]. The solution is accurate over the region with specified initial conditions and boundary conditions and is adequate for the computational purposes of this study.

The application of the integral method to the problem of the soil gas concentration profile involves three main assumptions. The first consists of the use of a polynomial function to define the concentration profile ($C_{z,t}$) of the i^{th} gas component in the compositional layer. The second assumes that the terms of the polynomial depend on the thickness of compositional layer (δ_t). The third assumption states that the polynomial's degree affects the accuracy of the solution. Because the terms of the polynomial are dependent on the thickness of the

compositional layer, a concentration profile term ($C_{z,t}$) must be introduced into equation (9). The solution of the ordinary differential equation provides the thickness of the compositional layer δ_t at a given time, thereby yielding the solution to the flux problem (equation 9).

To obtain the solution of equation (14) by applying the approximate integral method, the generic second-order polynomial

$$C = a+bz+cz^2 \tag{15}$$

is used because the solution accuracy is adequate to the purposes of this study. In accordance with the boundary conditions at z = 0 and z = δ_t (equations (11), (12), and (13)), the computation of the terms a, b, and c (Appendix 1) provides the following polynomial function:

$$C = \frac{J\delta+2DC_i}{\delta v+2D} - 2\frac{J-vC_i}{(v\delta+2D)}z + \frac{J-vC_i}{\delta(v\delta+2D)}z^2 \tag{16}$$

which describes the concentration profile of the i^{th} component in the soil (red curve in Figure 1).

The solution of equation (14), in accordance with the concentration profile of the i^{th} component (equation (16)), yields

$$3 = \frac{d}{dt}\left[\frac{\delta^2}{(v\delta+2D)}\right] \tag{17}$$

Equation (17) is subject to $\delta_t = 0$ for t = 0 and has the solution of δ:

$$\delta = \frac{\sqrt{3}(\sqrt{t(8D+3tv^2)}+\sqrt{3}tv)}{2} \tag{18}$$

which provides the thickness of the compositional layer as a function of time. The compositional perturbation commences at t = 0 from the lower limit of the soil and modifies the composition profile over the time interval

$$t_\delta = \frac{\delta^2}{6D+3\delta v} \tag{19}$$

which is the retention time (t_δ) of the i^{th} species under specific conditions, such as the soil thickness, permeability, flux rate and temperature. The calculation of the retention times (RT) for specific flux rates of different gas components is the term compared to the experimental results obtained from the laboratory experiments. According to equation (19), the RT of the i^{th} gas component depends on i) the thickness of the medium, ii) the gas velocity, and iii) the bulk diffusivity of the gas components. In the experimental system, the gas velocity and the thickness of the medium are both fixed. According to previous investigations (Reid et al., 1987), the diffusivity is a substance-dependent quantity and is a function of temperature and pressure. The difference in the bulk diffusivity (D) of the components of a gas mixture causes differences in the computed retention times. Therefore, a delay is predicted between the arrivals of the different gas species at the upper surface of a porous medium. The diffusivity values for many gases have been experimentally determined, and a comprehensive review of diffusivity as a function of temperature and pressure is available in *Marrero and Mason* [1972]. From a theoretical standpoint, a direct relationship exists between diffusivity and temperature, whereas an inverse relationship exists between the diffusion coefficients and pressure until the pressure drops below the critical pressure for the gas mixture, which is greater than 3 MPa for many gases. Further experimental determinations of the diffusivity for H_2, CO_2 and He are outside the scope of this study. However, the molecular diffusivities for CO_2, H_2, and He were estimated according to the theoretical method to evaluate the molecular diffusivity [*Chapman and Cowling*, 1970]. The computed D_i values (Table 1) for CO_2, He, and H_2 in excess of air were used in our model to predict the delays between the changes in CO_2 and H_2 for a wide range of temperatures. However, in the application of our theoretical values of diffusivity to the transport of gas mixtures through the soils, the actual diffusivity of CO_2, He and H_2 diverge from the computed D_i values because of the interaction among the gas components with large difference in molecular weight.

Figure 2 shows delays between changes in the concentrations of CO_2 and H_2 as a function of the advective flux rate (ν) at 0.1 and 1 MPa associated with changing the temperature from 293 to 1273 K. The results suggest that the delays computed at different flux rates increase as the temperature increases because the difference in the diffusivity of H_2 and CO_2 increases as a function of temperature. Accordingly, at a constant flux rate and temperature, the delays between CO_2 and H_2 decrease inversely with pressure. For the range of temperatures investigated from the theoretical perspective, we observed that, at a constant flux rate, the differences in the retention times of different components are on the order of hundreds of seconds (Figure 2). However, in the physical experiments, the tests were performed at 20 °C (293 K), and the effects of the slight changes in the environmental temperature on the delays between H_2 and CO_2 can be neglected. However, these changes are considered in the application of the theoretical model to the continuously monitored H_2 and CO_2 data from Etna volcano.

3. Laboratory experiments

To investigate the reliability of the theoretical model for the compositional changes in the soil gases, an experiment was designed and several tests were performed in the laboratory with a customized gas flux simulator (Figure 3). The experiments were carried out with CO_2, H_2 and He at 20 °C and under atmospheric pressure (an average pressure of 0.1 MPa).

The experimental equipment consisted of a cylindrical PVC pipe 280 cm high (referred to as flux column) with a circular cross-sectional area of 50.26 cm^2 (8 cm in diameter) and filled with dry volcanic sand collected from the present sea-shore deposits at Vulcano (Aeolian Archipelago). The permeability and the grain size of the sand were accurately determined in the laboratory.

Pure CO_2 (99.99 vol %) and pure He (99.99 vol %) were used as separate gas standards to

establish the gas flux in the column initially saturated with air. The results of these tests provided the RT under the conditions assumed by the theoretical model because the computation of the RT by equation (19) neglects the interaction effects among different gases and uses the binary diffusivity of the gas component in air. Furthermore, several laboratory gas standards, consisting of He, H_2, O_2, N_2, CO, CH_4, and CO_2 in different concentrations (Mix1, Mix2, Mix3, and Mix4), were also used to perform a specific set of flux tests. The compositions of the gas standards were determined in the laboratory by chromatographic analysis with a Perkin Elmer Clarus 500 with a Shincarbon ST 100/120 Mesh 3 m x 1/8" OD column (Table 2).

Several specific gas sensors (Table 3) were placed on top of the flux simulator to detect the different target gas components of the standard mixtures injected into the soil column. The response times of the sensors were 1 s for the He detector, 10 s for the CO_2 detector, and 20 s for the H_2 electrochemical sensor. The response time of each sensor was shorter than the expected RTs of the targeted gas species at the selected flux rates of each test. The sensors were connected to an acquisition computer through a DAC device, and the signals were sampled at 10 Hz (ten times faster than the shortest response time of the detectors).

The tests were performed at several flux rates between 10^{-3} and 10^{-1} $cm^3s^{-1}cm^{-2}$, which includes the empirical flux range typically measured in volcanic areas. The flux rates were fixed at the base of the column by manometers connected to the gas tank. A digital fluxmeter (Omega Engineering Inc FMA-114 with an accuracy of 2% for the full scale) was used to measure the flux rates up to 10^{-2} $cm^3s^{-1}cm^{-2}$; the flux rates above 10^{-2} $cm^3s^{-1}cm^{-2}$ were measured by a Ky Instrument variable area fluxmeter (range 0 - 0.33 $cm^3s^{-1}cm^{-2}$, with an accuracy of $1.66 \cdot 10^{-2}$ $cm^3s^{-1}cm^{-2}$). The fluxmeters were calibrated in the laboratory over the full flux range investigated, for measuring the gas flux of the gas standard (pure CO_2, pure He, and MGM standard) and mixtures (Mix1, Mix2, Mix3, and Mix4).

The tests consisted of recording the temporal changes in the concentration of the target gases in the upper part of the column after the gas was injected at the base of the column. From the experimental perspective, we assume that the retention time is the time when the concentration of the target gas at the top surface of the flux column is above the concentration baseline ($C_{initial}$).

The tests were completed a few minutes after the variation in the concentration was detected at the upper surface of the column. The duration of a test ranged from a few minutes to hours depending on the flux rate of the gas in the column. Throughout the tests, the atmospheric pressure and the temperature in the laboratory were also measured.

Air was used as the standard of the gas components' baseline concentrations in the porous medium of the column. Therefore, the cleaning procedure of the flux simulator involved flushing the column with air for several minutes before every procedure to measure the retention times.

4. Results

Figure 4 shows a typical record of a measurement of the retention times for a single-component gas (CO_2 or He). The gas enters at a constant flux rate from the base of the column, the gas sensor at the top surface measures the pristine concentration of the supplied gas species, and the slope of the signal-time curve is zero. The slope of the signal-time curve increases as the gas flux modifies the compositional profile in the column. According to the statistical evaluation of the voltage data over the first 300 seconds of signal recording (both average and standard deviation), the time at which the difference between the effective signal and the average voltage exceeded steadily the variance of the base signal has been selected as retention time of the gas species.

4.1.Tests with pure CO_2

Several tests were performed in the laboratory with pure CO_2 (99.99 vol %) because CO_2 is the predominant component (along with water) in volcanic gases. A Gascard II IR spectrophotometer was used to detect the CO_2 at the upper surface of the flux column. Table 4 lists the experimental RT ($t_{measure}$) and the computed RT (t_{model}) for the tests performed with selected flux rates (v) in the range 0.004 - 0.332 $cm^3s^{-1}cm^{-2}$.

Figure 5 shows the comparison between the RT measured for CO_2 ($t_{measure}$) as a function of the flux rate (v) of the gas in the column and the theoretical RT predicted by equation (19). The error bars were computed in accordance with the accuracy of the flux rate measurements and the response time of the CO_2 sensor.

According to the experimental accuracy, the figure indicates a good correspondence between the experimental data obtained with pure CO_2 and the theoretical computations across the full range of the flux rates investigated.

4.2. Tests with pure He

An evaluation of the retention times of H_2 as a single component was performed with pure He (99.99 vol %). He was used as the gas standard because its atomic weight (AW_{He} = 4 amu) and its diffusivity in air ($D_{He\text{-}Air}$ = 0.58 cm^2s^{-1}) are similar to the molecular weight and diffusivity of H_2 (MW_{H_2} = 2 amu; $D_{H_2\text{-}Air}$ = 0.67 cm^2s^{-1}). Both parameters are very different from the diffusivity and molecular weight of CO_2.

During the laboratory experiments, an Alcatel ASM 100 HDS mass spectrometer (Table 3) was used to measure the variations in the He concentration at the upper surface of the flux column. Table 5 lists the experimental RT ($t_{measure}$) and the computed RT (t_{model}) for the tests carried out with pure He.

The theoretical RT for He (black curve) was computed with equation (19) for a flux rate

range of 0.03 - 0.35 $cm^3s^{-1}cm^{-2}$, and the measurements of the RT were performed for thirteen selected He flux rates (Figure 6).

The experimental results for He indicate that the theoretical RTs agree with the experimental data across the full range of investigated flux rates in the limit of the experimental accuracy. As discussed in the following, the experimental RTs are lower than the theoretical RTs because of the high kinematic viscosity of the He. As observed with pure CO_2, the results obtained from the tests performed with He as a single component indicate that the theoretical model accounts for the composition changes in the ground gases within the limits of the experimental accuracy.

4.3.Tests with multicomponent mixtures

The simultaneous measurements of the RTs of H_2 and CO_2 were performed using several multicomponent gas mixtures (MGM). The composition of the mixtures (Table 2) consisted of He, H_2, O_2, N_2, CO, CH_4, and CO_2. The tests were performed with the MGM standard (Table 2) at seventeen different flux rates in the range 0.004 – 0.332 $cm^3s^{-1}cm^{-2}$. A City Technology electrochemical sensor and a Gascard II IR spectrophotometer (Table 3) were used to detect changes in both the H_2 and CO_2 concentrations at the upper surface of the flux column.

A typical record of the tests involving the multicomponent standards is shown in Figure 7. Following time zero, the gas flowed into the column at a fixed flux rate. The H_2 concentration at the top of the column changed noticeably several minutes earlier than the CO_2 concentration. The MGM standard modified the CO_2 concentration profile after the change in the H_2 concentration. The time difference between the retention times of CO_2 and H_2 is referred to as the CO_2–H_2 delay. Table 6 lists the experimental RTs of CO_2 and H_2 with the theoretically calculated RTs at selected flux rates.

The experimental retention times of CO_2 and H_2 obtained by using the MGM standard are reported as functions of the flux rate in Figures 8a and 8b, respectively. In these graphs, the theoretical retention times of both CO_2 and H_2, calculated using equation (19), are also depicted (black lines in Figures 8a and 8b, respectively). Similar to the pure CO_2 experiments, the predictions of the theoretical model correspond to the experimental RTs for flux rates larger than 0.060 $cm^3s^{-1}cm^{-2}$ for the CO_2 with the MGM standard (Figure 8a). For flux rates up to 0.053 $cm^3s^{-1}cm^{-2}$, the experimental CO_2 RTs were systematically longer than the theoretical computations. The largest differences were observed for low flux rates. Similarly, the theoretical H_2 RTs (black curve in Figure 8b) agree with the experimental results (red diamonds) for flux rates greater than 0.053 $cm^3s^{-1}cm^{-2}$, whereas large differences are present at lower flux rates. In the range of lower flux rate, the experimental data reveal the effect of the addition of multiple components to the gas flows results in the mutual and symmetric deceleration of each component (Figure 8). The difference between experimental and theoretical RTs is consistent with multicomponent effects of the gas components in the transport through the porous medium. Therefore, the effects of the mixture composition in the resulting RT have to be considered during the transport process of the gas through the porous media. The H_2 RTs for the tests performed at flux rates less than 0.046 $cm^3s^{-1}cm^{-2}$ were systematically shorter than the theoretical computations (Figure 8b).

The results indicate differences between the theoretical predictions and the experimental RTs for CO_2 and H_2 when the diffusive component of the gas flux is dominant. This pattern results from the large difference in diffusivity between CO_2 and H_2: the diffusivity of H_2 is significantly greater than the diffusivity of CO_2. As discussed in the following sections, the differences between the theoretical conclusions and the experimental data result from the diffusive component of the gas transport process through the porous medium. This discrepancy can be corrected by using appropriate diffusivity values for each gas species.

4.4. Effects of the mixture composition

The MGM standard is a complex mixture of He, H_2, O_2, N_2, CO, CH_4, and CO_2, and the effects of the mixture composition on the RTs of H_2 and CO_2 were evaluated in the laboratory through a set of tests with several gas standards with intermediate compositions between the MGM standard and pure CO_2 (Table 2). The tests were performed at a constant flux rate of 0.027 $cm^3s^{-1}cm^{-2}$ and repeated at 0.04 $cm^3s^{-1}cm^{-2}$ (Figure 9). The results of the tests indicate that the retention times of both CO_2 and H_2 change as functions of the pristine mixture compositions. The main differences between the theoretical RTs and the experimental data were observed with the MGM standard, whereas the theoretical predictions replicate the experimental RTs of H_2 and CO_2 measured with Mix4. Furthermore, the results of the experiments indicate that the theoretical RTs of CO_2 replicate the effective RTs because the CO_2 concentration in the gas mixture is greater than 40 vol % and the trend is independent of the flux rate. Accordingly, the RT of H_2 increases as a function of the CO_2 concentration. The theoretical computation of the RTs reproduces the experimental results for H_2 because the concentration of H_2 is on the order of hundreds of ppm by volume, at least in the case of the test performed at 0.04 $cm^3s^{-1}cm^{-2}$. As observed for CO_2, the trend in the retention times for H_2 as a function of the mixture's composition is independent of the flux rate applied.

4.5.Effects of soil thickness

The measurements of the RTs allow us to compute the delays in the concentration changes in CO_2 and H_2. According to the theoretical model, these delays are a function of the length of the flux column, which corresponds to the depth of the gas source in the reference frame of volcanic systems. Therefore, the connection between the retention times and the distance between the gas source and the detectors was targeted through a set of specific tests. The tests were performed with Mix4 at a constant flux rate of 0.006 $cm^3s^{-1}cm^{-2}$, and the RTs were

measured for CO_2 and H_2. The five measurements of the RTs were performed at different distances from the gas source, with the detectors connected to the special openings in the flux column (black-points in Figure 3). The results of these tests are shown in Figure 10 (green diamonds for CO_2 in Figure 10-a and blue diamonds for H_2 in Figure 10-b, respectively). The high value of the correlation coefficient indicates a rectilinear relationship between the RT and the thickness of the porous medium for both the CO_2 and H_2 components. This linearity is a very important result for the purposes of this investigation and suggests that the delays between the CO_2 and H_2 changes (Figure 10-c) are well described by a linear relationship through the origin ($R^2 = 0.998$) across the full range of distances investigated. This feature of the fitting line supports the experimental evidence that both components are mixed at the start of the tests and that the delay between the CO_2 and H_2 is zero at the gas inlet. Therefore, the delays between the CO_2 and H_2 changes are derived from the flux through the porous medium, directly related to the thickness of the transited rocks, and result from the diffusive component of the advective-diffusive gas transport process.

5. Discussion

CO_2, H_2 and He were used to study asynchronous changes in the compositions of soil gases because they differ significantly in diffusivity and are representative of the gas components emitted by soils in volcanic areas. Our simplified theoretical model of the gas transport through a porous medium and the gas flux experiments performed in the laboratory suggest that the evolution of the CO_2 and H_2concentrations in the soil gases is related to the depth of the gas source.

Data obtained using pure CO_2 and pure He indicated that the theoretical computations replicate the experimental results across the full range of the studied flux rates. These data are strongly supportive of the theoretical model for predicting the RTs of a single gas component

moving through the soil. However, certain differences were observed between the theoretical calculations and the experimental data for CO_2 and H_2 obtained using the MGM standard at flux rates lower than 0.053 $cm^3s^{-1}cm^{-2}$ (Figure 8). In that flux range, the experimental data deviate from the theoretical prediction as a function of the pristine composition of the gases, and the CO_2 RTs are systematically longer than the experimental RTs measured with pure CO_2. These differences result from the diffusive component of the mass and momentum transfer during the gas transport process through the soils. In fact, the theoretical calculations replicate the experimental results for pure CO_2 and pure He because the binary diffusion coefficient of CO_2 and He in air represents the actual diffusivity of both the components in the flux column. The same values of the bulk diffusion coefficients were used in the computation of the RTs for both H_2 and CO_2 with the MGM standard, in which multicomponent effects can influence the diffusion processes. According to *Cussler* [1997], the multicomponent effects are larger when the mixture is concentrated or contains interacting species. These interactions originate from chemical reactions, electrostatic coupling or large differences in molecular weights of the mixture components, which is the case for CO_2 and H_2. Furthermore, both the density and dynamic viscosity of the flowing mixture are affected by the chemical composition of the gases. Therefore, the chemical composition of the mixture affects the kinematic viscosity of the gas mixture, which is the ratio between the density and the dynamic viscosity. The kinematic viscosity is an indicator of the ability of the gas to transport momentum; this parameter has the same dimensions as molecular diffusivity ($L^2\ t^{-1}$, where L is a convenient length scale and t is time) and relates the momentum flux to the velocity gradient. During the experiments of gas transport through soil, both the molecular diffusivity and kinematic viscosity of the gas mixture in the column change over time because of the different diffusivities of the components in the MGM standard. By considering the effects of the changes in the composition of the flowing mixture

on the H_2 and the CO_2 separately, the kinematic viscosity of the gas changes from that of the MGM standard (1.514 mPa · s) to that of pure H_2 (10.505 mPa · s) and results in a gain of momentum diffusion for H_2. Because the whole momentum is preserved during transport, the change in the kinematic viscosity of the flowing mixture produces a loss of momentum diffusion for CO_2 because the kinematic viscosity of pure CO_2 (0.782 mPa · s) is lower than that of the MGM standard. A loss in momentum and molecular diffusivities results in a decrease in the effective flux velocity for CO_2. In contrast, the increase in momentum and molecular diffusivities results in an increase in the effective flux velocity for H_2. Accordingly, in the lower flux range ($v < 0.053$ $cm^3s^{-1}cm^{-2}$), the diffusive component of the mass transfer is dominant, and the RTs of CO_2 associated with the MGM standard are longer than both the RTs associated with pure CO_2 and the theoretical computations (light blue diamonds in Figure 11). Furthermore, the experimental retention times of H_2 are lower than the theoretical predictions (red diamonds in Figure 11).

Because the integral method provides an accurate solution of the flux problem in an average sense, the application of the theoretical predictions justify a reasonable tolerance in the use of averaged values for the flux parameters that are different from those reported in the catalogues. The experimental data obtained in the laboratory indicate that the measured RTs agree with the theoretical predictions when the flux parameters of the mixture change by approximately 20 % due to the differences in the diffusivity of the components and the evolution over time in the kinematic viscosity of the flowing mixture (dashed lines in Figure 11).

The dependency on the length of the flux column supports the inference that the continuous monitoring of the ground gases in volcanic areas provides insights into the depth of the reservoir via the evaluation of the delay between two or more gas components. The theoretical model and the experimental data indicate that the complex mixture released from

the gas source at depth produces asynchronous changes in the composition of the gas emitted by soils. The gas separation process of the pristine mixture during transport produces a delay between the changes in the concentrations of different components. The delays are a function of the differences in the actual diffusivity of the gas species, the flux rate, and the depth of the gas source. From this perspective, H_2 and the CO_2 can be treated as proxies for the depth of the source because of the large differences in their diffusivities.

Both theoretical and experimental results were applied to study the delay between CO_2 and H_2 changes recorded at Etna volcano via the continuous monitoring of the ground gases [*Di Martino et al*., 2013]. The data were collected at the Belvedere site (Figure 12c), situated in a low-temperature fumarolic field (T < 100 °C) at the edge of the Valle del Bove on the eastern flank of the volcano. At Belvedere, the period between end of July and September 2010 was characterized by anomalous values for both the volcanic gas components, and the changes in the H_2 concentration preceded the changes of the CO_2 concentration [*Di Martino et al*., 2013]. To analyze the data on the delays associated with changes in H_2 and CO_2, the raw time series were down-sampled using a moving average with a 17-hour window. The average values were attributed to the ninth hour, and the resulting time series were studied (Figure 12a). The advantage of this central−difference method is that it does not involve a shift in the time−axis position of the average value of both CO_2 and H_2 measurements. Furthermore, the 8 hours time window at left and right of the middle 9^{th} hour removes from the signals the pumping effect on the soil gases [*Massman and Farrier*, 1992; *Hinkle*, 1994; *Chiodini et al.*, 1998; *Massman*, 2006; *Rinaldi et al.*, 2012] induced by daily cycles of the atmospheric pressure. The peak CO_2 values were compared with the H_2 peaks, the delays between the CO_2 peaks relative to the H_2 peaks were computed, and the positive delay values between the CO_2 and H_2 peaks were considered. The frequency histogram of the entire delay dataset (Figure 12-b) indicates that the most frequent value for the delay between changes in CO_2 and H_2 was

293 hours during the study period. The average CO_2 flux in this time interval was approximately 1100 g m^{-2} d^{-1} [*Di Martino et al.,* 2013], and this value was used as the average flux rate for the application of the theoretical model. In an attempt to investigate the depth of the degassing source, the diffusivity of both H_2 and CO_2 was computed at 100 °C and 0.08 MPa, which are the average values for temperature and atmospheric pressure measured at the sampling site. Based on these data, the theoretical computation yielded a distance to the degassing source of 2200 - 2300 meters below the measurement site. Taking into account the topographic elevation of the Belvedere (approximately 2800 m.a.s.l.), we argue that the H_2 and CO_2 start to move by following an advective-diffusive transport processes from an average elevation of 500 – 600 m.a.s.l. This depth to the degassing source in the volcanic edifice agrees with the maximum depth observed for the source of the volcanic tremor, which has been estimated by independent geochemical and geophysical investigations [*Aiuppa et al.,* 2010b; *Andronico et al.,* 2013]. Moreover, the delay intervals between the H_2 and CO_2 peaks shorter than the most frequent value of 293 hours (Figure 12-b) are consistent with the degassing source moving toward shallower levels during the increase in volcanic activity. From the other hand, at least some of the observed delays larger than the most frequent value are consistent with the inference of a H_2-bearing CO_2-rich gas mixture moving from deepest portion of the plumbing system of the Etna volcano during the current persistent degassing activity (Figure 12-d).

Although a sort of chromatographic effect has been reported for CO_2 and CH_4 monitoring in fumaroles [*Chiodini et al.,* 2009] and we have yet to generalize the results reported in this paper for different volcanic systems, the theoretical results, experimental data, and application of the theoretical model to the data collected at Etna volcano via the continuous monitoring of H_2 and CO_2 strongly support the relevance of investigating the connection between the evolution of the chemistry of the ground gases and the depth of the gas reservoir.

Moreover, the gas separation results from the gas dispersion through the porous media, and have to be expected in most systems, even more in the systems with deep sources. Therefore, the monitoring of multiple gas components mainly those with sensitive differences in diffusivity (e.g. CO_2 and He or CO_2 and H_2) by continuous monitoring systems or periodic surveys, could constraint the depth the gas sources in volcanic and non volcanic areas. However, long time series analysis can provide supportive information, because of each single observation (e. g. by measuring CO_2/He or CO_2/H_2 ratios) can be representative of a transient state, rather than of a steady or equilibrium state of the system.

6. Conclusions

This paper focuses on the relationship between asynchronous changes in the composition of volcanic gases and the depth of the gas source by advancing a simplified theoretical model of the gas transport through the soils and performing a set of laboratory experiments. Our theoretical model accounts for the advective-diffusive transport processes of the i^{th} gas component through the soil. The experiments were performed with a gas flux simulator to investigate the chemical composition changes in the volcanic gases as function of the gas flux, the composition of the pristine mixture, pressure, temperature, and the depth of the gas source. These experiments were used to check the accuracy and the limits of validity of the theoretical conclusions.

In the reference frame of a volcanic environment, the theoretical approach models the time period between a gas release from a source at depth and the identification of compositional changes in the soil gases at the surface. This period is referred to as the retention time (RT).

The results of the experiment indicated that the theoretical computations replicate the experimental RTs of both pure CO_2 and pure He across the full range of the studied flux rates.

Both the analytical results and the experimental data indicate that the gas transport through the rocks tends to separate the components of the complex mixture as the flux rate decreases, producing asynchronous changes in the chemical compositions of the volcanic gases.

Several tests were performed with gas mixtures composed of He, H_2, O_2, N_2, CO, CH_4, and CO_2. The results of these tests allowed us to measure the differences between the experimental RTs and the theoretical computations for CO_2, and H_2. The experimental data indicated that the effects of the mixture's composition on the diffusivity of both mass and momentum of the gas components account for the differences between the theoretical calculations and the experimental RTs for CO_2 and H_2.

The results of the tests on valid compositional ranges for the theoretical approach indicate that the model replicates the experimental RTs of CO_2 and H_2 in CO_2-rich gas mixtures (CO_2 > 40 vol %) with trace amounts of H_2 (hundreds of ppm vol). Such mixtures represent the typical composition of gases emitted in volcanic and geothermal areas.

Our experimental data reveal a linear relationship between the delays in the retention times of different gas components and the thickness of the traversed rocks. In the framework of volcanic and geothermal environments, this linearity suggests that the investigation of the delays in the changes of two or more volcanic gas components with large differences in diffusivity provides a relationship between the chemistry of the volcanic gases and the depth of the gas source. The application of the theoretical model to the data collected by the continuous monitoring of the low-temperature fumaroles at Etna volcano provides a depth for the degassing source that is consistent with the maximum depth of the source of the volcanic tremor.

Acknowledgements

The authors are grateful for useful suggestions and constructive comments by associate editor

André Revil and an anonymous reviewer which improved the original manuscript.

The data for this paper are available by contacting the corresponding author at robertomr.dimartino@gmail.com

APPENDIX 1

Derivation of the coefficients of Equation (16)

To obtain the *a*, *b* and *c* terms of the equation (15) ($C = a + bz + cz^2$) we use the boundary condition expressed in the theoretical model and summarised as follow:

$$-D\frac{dC}{dz}+\nu C=J \quad \text{at} \quad z = 0 \tag{11}$$

$$\frac{dC}{dz}=0 \tag{12}$$

$$C=C_i \tag{13}$$

In accordance with equation (11), at $z = 0$

$$C = a+bz+cz^2$$

$$C = a$$

and

$$-Db+\nu a = J .$$

Therefore

$$a = \frac{J+Db}{\nu} \tag{20}$$

At $z = \delta$, in accordance with the boundary condition (12)

$$b+2c\delta = 0$$

or

$$b = -2c\delta \tag{21}$$

and, from (13)

$$C_i = a+b\delta+c\delta^2$$

$$c = \frac{C_i - a - b\delta}{\delta^2} \tag{22}$$

Following equation (20), equation (21), and equation (22), the *c* term of the polynomial function is computed as

$$c = \frac{1}{\delta^2}\left[C_i - \frac{J+D(-2c\delta)}{\nu} - (-2c\delta)\delta \right]$$

This results in

$$c = \frac{J-\nu C_i}{\delta(\nu\delta+2D)} \tag{23}$$

Placing (23) into the equation (21) provides

$$b = -2\left[\frac{J-\nu C_i}{(\nu\delta+2D)} \right] \tag{24}$$

and (24) into (20) provides the *a* term of (15)

$$a = \frac{1}{\nu}\left[J+D\left(-2\frac{J-\nu C_i}{(\nu\delta+2D)} \right) \right]$$

or

$$a = \frac{J\delta+2DC_i}{\delta\nu+2D} \tag{25}$$

Equations (23), (24), and (25) provide the polynomial function

$$C = \frac{J\delta+2DC_i}{\delta\nu+2D} - 2\frac{J-\nu C_i}{(\nu\delta+2D)}z + \frac{J-\nu C_i}{\delta(\nu\delta+2D)}z^2 \tag{16}$$

This now describes the concentration profile of the i^{th} component in the porous medium.

References

Aiuppa, A., C. Federico, G. Giudice, and S. Gurrieri (2005), Chemical mapping of a fumarolic field: La Fossa Crater, Vulcano Island (Aeolian Islands, Italy), *Geophys. Res. Lett.*, 32, L13309, doi:10.1029/2005GL023207.

Aiuppa, A., G. Giudice, S. Gurrieri, M. Liuzzo, M. Burton, T. Caltabiano, A. J. S. McGonigle, G. Salerno, H. Shinohara, and M. Valenza (2008), Total volatile flux from Mount Etna, *Geophys. Res. Lett.*, *35*, L24302, doi:10.1029/2008GL035871.

Aiuppa, A, C. Federico, G. Giudice, G. Giuffrida, R. Guida, S. Gurrieri, M. Liuzzo, R. Moretti, and P. Papale (2009), The 2007 eruption of Stromboli volcano: Insights from real-time measurement of the volcanic gas plume CO_2/SO_2 ratio, *J. Volcanol. Geoth. Res.*, *182*, 221-230, doi:10.1016/j.jvolgeores.2008.09.013.

Aiuppa, A., A. Bertagnini, N. Métrich, R. Moretti, A. Di Muro, M. Liuzzo, and G. Tamburello (2010a), A model of degassing for Stromboli volcano, *Earth Planet. Sc. Lett.*, *295*, 195–204, doi:10.1016/j.epsl.2010.03.040.

Aiuppa, A., A. Cannata, F. Cannavò, G. Di Grazia, F. Ferrari, G. Giudice, S. Gurrieri, M. Liuzzo, M. Mattia, P. Montalto, D. Patanè, and G. Puglisi (2010b), Patterns in the recent 2007-2008 activity of Mount Etna volcano investigated by geophysical and geochemical observations, *Geochem. Geophys. Geosyst.*, 11(9), Q09008, doi:10.1029/2010GC003168.

Andronico, D., M. D. Lo Castro, M. Sciotto, and L. Spina (2013), The 2010 ash emissions at the summit craters of Mt Etna: Relationship with seismo-acustic signals, *J. Geophys. Res.*, 118, 51–70, doi:10.1029/2012JB009895.

Aubert, M. (1999), Practical evaluation of steady heat discharge from dormant active volcanoes: case study of Vulcarolo fissure (Mount Etna, Italy), *J. Volcanol. Geoth. Res.*, *92*, 413–429, doi: 10.1016/S0377-0273(99)00088-8.

Berkowitz, B. (2002), Characterizing flow and transport in fractured geological media: a review, *Adv. Water Resour.*, *25*, (8-12), 861–884, doi: 10.1016/S0309-1708(02)00042-8.

Camarda, M., S. Gurrieri, and M. Valenza (2006), CO_2 flux measurements in volcanic areas using the dynamic concentration method: Influence of soil permeability, *J. Geophys. Res.* 111, B05202, doi: 10.1029/2005JB003898.

Camarda, M., S. De Gregorio, R. Favara, and S. Gurrieri (2007), Evaluation of carbon isotope fractionation of soil CO_2 under an advectie-diffusive regimen: a tool for computing the isotopic composition of unfractionated deep source, *Geochim. Cosmochim. Ac.*, 7, 3016–3027, doi: 10.1016/j.gca.2007.04.002

Camarda, M., S. De Gregorio, and S. Gurrieri (2012), Magma-ascent processes during 2005-2009 at Mt Etna inferred by soil CO_2 emissions in peripheral areas of the volcano, *Chem. Geol.*, 330–331, 218–227, doi: 10.1016/j.chemgeo.2012.08.024.

Capasso, G., G. Dongarrà, R. Favara, S. Hauser, and M. Valenza (1992), Isotope composition of rain water, well water and fumarole steam on the Island of Vulcano, and their implications for volcanic surveillance, *J. Volcanol. Geoth. Res.*, 49(1-2), 147–155.

Carslaw, H. S., and J. C. Jaeger (1959), Conduction of Heat in Solids, Oxford University Press, USA, ISBN: 9780198533030.

Chapman, S., and T. G. Cowling (1970), The mathematical theory of non−uniform gases, 3rd Ed, Cambridge Mathematical Library, ISBN: 978-0521408448.

Cheng, A. H. D., and D. T. Cheng (2005), Heritage and early history of the boundary element method, *Eng. Anal. Bound. Elem.*, 29, 268–302, doi: 10.1016/j.enganabound.2004.12.001.

Chiodini, G., R. Cioni, M. Guidi, L. Marini, and B. Raco (1998). Soil CO_2 flux measurements in volcanic and geothermal areas. *Appl. Geochem.*, *13*(5), 543–552, doi:10.1016/S0883-2927(97)00076-0

Chiodini, G., F. Frondini, C. Cardellini, D. Granieri, L. Marini, and G. Ventura, (2001), CO_2 degassing and energy release at Solfatara volcano, Campi Flegrei, Italy. *J. Geophys. Res.*

106(B8), 16213–16221, doi:10.1029/2001JB000246.
Chiodini, G., D. Granieri, R. Avino, S. Caliro, A. Costa, and C. Werner (2005), Carbon dioxide diffuse degassing and estimation of heat release from volcanic and hydrothermal systems. *J. Geophys. Res.*, 110, B08204, doi:10.1029/2004JB003542.
Chiodini, G. (2009), CO_2/CH_4 ratio in fumaroles a powerful tool to detect magma degassing episodes at quiescent volcanoes, *Geophys. Res. Lett.*, *36*, L02302, doi:10.1029/2008GL036347.
Cussler, E. L. (1997), *Diffusion: Mass transfer in fluid systems*, Cambridge Series in Chemical Engineering 2nd ed., 600 pp., Cambridge University Press.
De Gregorio, S., M. Camarda, S. Cappuzzo, and S. Gurrieri (2013), An innovative method for continuous measurement of soil CO_2 flux, *Chem. Geol.*, *341*, 102–109, doi: 10.1016/j.chemgeo.2013.01.011.
Di Martino, R. M. R., M. Camarda, S. Gurrieri, and M. Valenza (2013), Continuous monitoring of hydrogen and carbon dioxide at Mt Etna, *Chem. Geol.*, *357*, 41–51, doi:10.1016/j.chemgeo.2013.08.023.
Epstein, N. (1989), On tortuosity and the tortuosity factor in flow and diffusion through porous media. *Chem. Eng. Sci.*, *44*(3), 777–779.
Gerlach, T. M., M. P. Doukas, K. A. McGee, and R. Kessler (2001), Soil efflux and total emission rates of magmatic CO_2 at the Horseshoe Lake tree kill, Mammoth Mountain, California, 1995– 1999, *Chem. Geol.*, 177, 101–116.
Giammanco, S., S. Gurrieri, and M. Valenza (1995), Soil CO_2 degassing from the ground on mount Etna during 1992, *Acta Vulcanol.*, *6*, 7–9.
Giammanco, S., S. Inguaggiato, and M. Valenza (1998), Soil and fumarole gases of Mount Etna: geochemistry and relations with volcanic activity, *J. Volcanol. Geoth. Res.*, *81*, 297–310.
Giggenbach, W.F. (1987), Redox processes governing the chemistry of fumarolic gas discharges from White Island, New Zeland, *Appl. Geochem.*, *2*, 143–161.
Granieri, D., R. Avino, and G. Chiodini (2009), Carbon dioxide diffuse emission from the soil: ten years of observations at Vesuvio and Campi Flegrei (Pozzuoli), and linkages with volcanic activity, *Bull. Volcanol.*, *72*, 103–118.
Gurrieri, S., M. Liuzzo, and G. Giudice (2008), Continuous monitoring of soil CO_2 flux on Mt. Etna: The 2004–2005 eruption and the role of regional tectonics and volcano tectonics, *J. Geophys. Res.*, *113*, B09206, doi:10.1029/2007JB005003.
Hardee, H.C. (1982), Permeable convection above magma bodies, Tectonophysics, *84*(2-4), 179-195, doi:10.1016/0040-1951(82)90159-7.
Hinkle, M. E. (1994), Environmental conditions affecting He, CO_2, O_2, and N_2 in soil gases, *Appl. Geochem.*, 9, 53–63.
Ho, C. K., and S. W. Webb (2006), Gas transport in porous media, in Theory and applications of transport in porous media, vol 20, Springer Netherlands, doi:10.1007/1-4020-3962-X.
Isachenko, V., V. Osipova, and A. Sukomel (Eds.) (1980), Heat Transfer, 493 pp. Mir, Moscow.
Jury, W. A., W. F. Spencer, and W. J. Farmer (1983), Behavior assessment model for trace organics in soil: 1, model description, *J. Environ. Qual.*, *12*, 558–564.
Klaseboer, E., Q. Sun, and D. Y. C. Chan (2012), Non-singular boundary integral methods for fluid mechanics applications, *J. Fluid Mech.*, *969*, 468–478, doi: 10.1017/jfm.2012.71.
Köhne, J. M., S. Köhne, and J. Šimůnek (2009), A review of model applications for structured soils: b) Pesticide transport, *J. Contam. Hydrol.*, *104*, 36–60, doi:10.1016/j.jconhyd.2008.10.003.
Marrero, T. R., and E. A. Mason (1972), Gaseous diffusion coefficients, *J. Phys. Chem. Ref.*

Data, 1.
Massman, J., and D. F. Farrier (1992), Effect of atmospheric pressure on gas transport in the vadose zone, *Water Resour. Res.*, *28*(3), 777–791, doi:10.1029/91WR02766.
Massman, W. J. (2006), Advective transport of CO_2 in permeable media induced by atmospheric pressure fluctuations: 1. An analytical model, *J. Geophys. Res.*, *111*(G3), doi:10.1029/2006JG000163.
Ptak, T., M. Prapenbrink, and E. Martac (2004), Tracer tests for the investigation of heterogeneous porous media and stochastic modeling of flow and transport – A review of some recent developments, *J. Hydrol.*, *294*(1), 122–163, doi:10.1016/j.jhydrol.2004.01.020.
Reid, R. C., J. M. Prausnitz, and B. E. Poling (1987), The properties of gases and Liquids, 4th ed., McGaw-Hill, New York.
Rinaldi, A. P., J. Vandemeulebrouck, M. Todesco, and F. Viveiros (2012), Effect of atmospheric conditions on surface diffuse degassing, *J. Geophys. Res.*, 117, B11201, doi:10.1029/2012JB009490.
Roberts, T. J., C. F. Braban, C. Oppenheimer, R. S. Martin, R. A. Freshwater, D. H. Dawson, P. T. Griffiths, R. A. Cox, J. R. Saffell, and R. L. Jones (2012), Electrochemical sensing of volcanic gases, *Chem. Geol.*, *332-333*, 74–91, doi: 10.1016/j.chemgeo.2012.08.027.
Sahimi, M., G. R. Gavalas, and T. T. Tsotsis (1990), Statistical and continuum models of fluid-solid reactions in porous media, *Chem. Eng. Sci.*, *45*(6), 1443–1502.
Sahimi, M., (1995), Flow and Transport in Porous Media and Fractured Rock: From Classical Methods to Modern Approaches,VCH Publisher, New York.
Shinohara, H. (2005), A new technique to estimate volcanic gas composition: plume measurements with a portable multi-sensor system, *J. Volcanol. Geoth. Res.*, *143*(4), 319-333, doi:10.1016/j.jvolgeores.2004.12.004.
Shinohara, H., A. Aiuppa, G. Giudice, S. Gurrieri, and M. Liuzzo (2008), Variation of H_2O/CO_2 and CO_2/SO_2 ratios of volcanic gases discharged by continuous degassing of Mount Etna volcano, Italy, *J. Gephys. Res – Sol. Ea.*, *113*, B09203, doi:10.1029/2007JB005185.
Sleep, B. E. (1998), Modeling transient organic vapor transport in porous media with the dusty gas model, *Adv. Water Resour.*, *22*(3), 247–256, doi:10.1016/S0309-1708(98)00011-6.
Taylor, A. W., and W. F. Spencer (1990), Volatilization and vapor transport processes in pesticides in the soil environment: processes, impacts and modeling, *Soil Sci. Soc. Am.*, *2*, 213–269.
Werner, C., S. L. Brantley, and K. Boomer (2000), CO_2 emission related to the Yellowstone volcanic system: 2. Statistical sampling, total degassing, and transport mechanisms, *J. Geophys. Res*, 105(B5), 10831–10846, doi:10.1029/1999JB900331.
Wu, Y. S., and K. Pruess (2000), Integral solutions for transient fluid flow through a porous medium with pressure-dependent permeability, *Int. J. Rock Mech. Min.*, 37, 51–61.
Yates, S. R., S. K. Papiernik, I. Gao, and J. Gan (2000), Analytical solutions for the transport of volatile organic chemicals in unsaturated layered systems, *Water Resour. Res.*, *36*(8), 1993–2000.

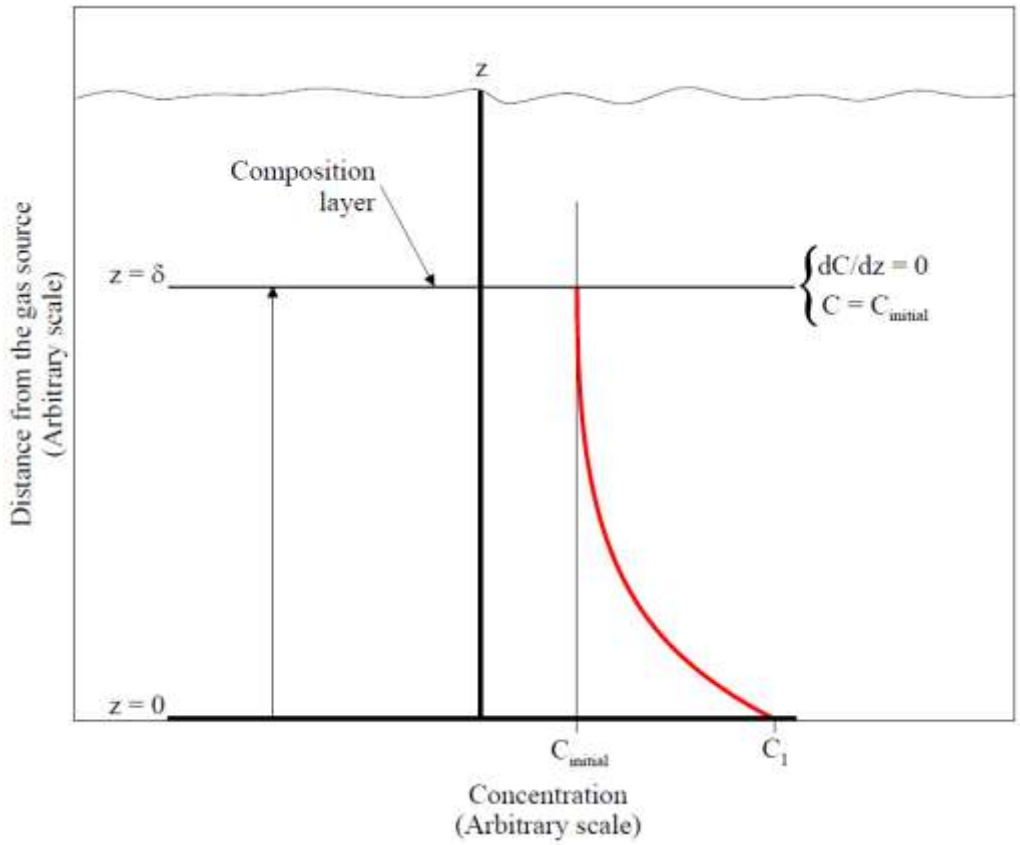

Figure 1. Picture of the composition layer (δ) defined by Equation [12], and Equation [13]. The red line indicates the second order polynomial function that describes the concentration profile of the i^{th} component in the porous medium. C_1 is the concentration of the i^{th} component in the gas standard. The z axis indicates the gas flux direction.

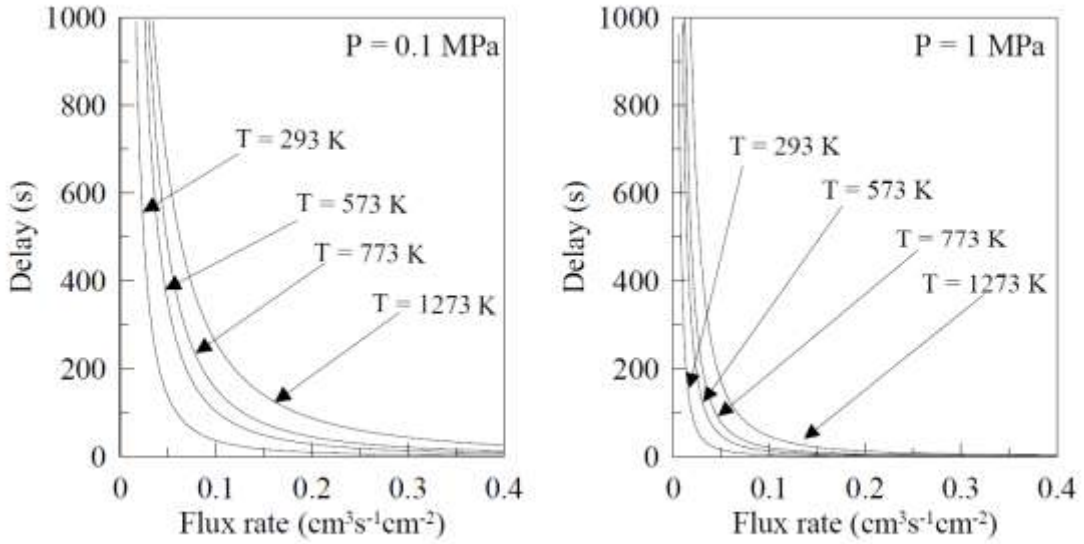

Figure 2. Computed delay between the CO_2 and the H_2 concentration transients as function of the flux rate. The theoretical curves of the delay were computed for different temperature at pressure of a) 0.1 MPa and b) 1MPa.

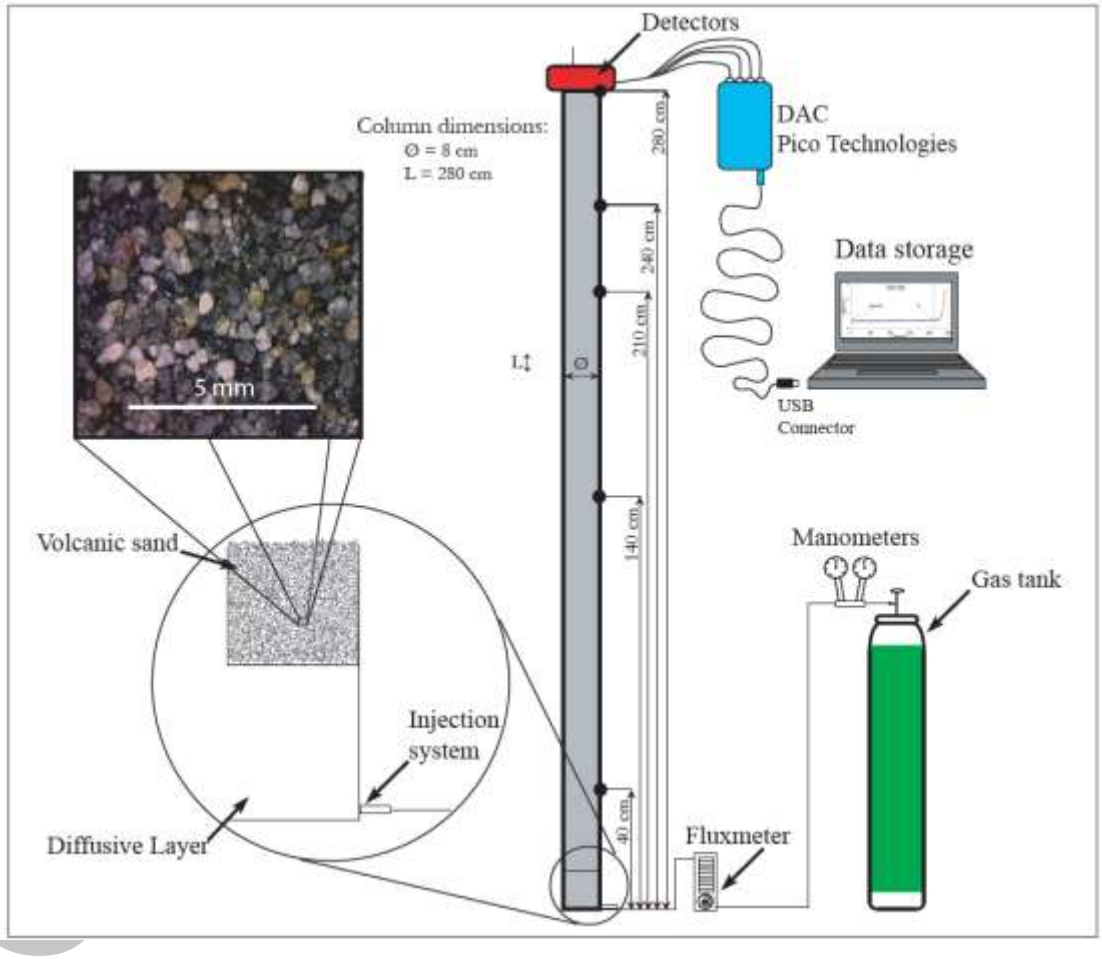

Figure 3. Laboratory-scale gas flux simulator for the experimental study of the transient in the soil gases. The flux column consist of a PVC cylindrical container 8 cm in diameter (cross section area 50.26 cm^2) 280 cm high (L), filled with volcanic sand (scaling up 200x in the box) collected from the present sea-shore deposits at Vulcano (Aeolian archipelago). The tank of the gas standards is connected to the flux column by the manometers, the silicone tubing, and the fluxmeter. The system of detectors measures the concentration of CO_2, H_2, and He. The gas sensors are connected with an acquisition computer to record the evolution of the concentrations of the target components at the upper surface of the column. The sampling frequency of the gas sensor signals was 10 Hz.

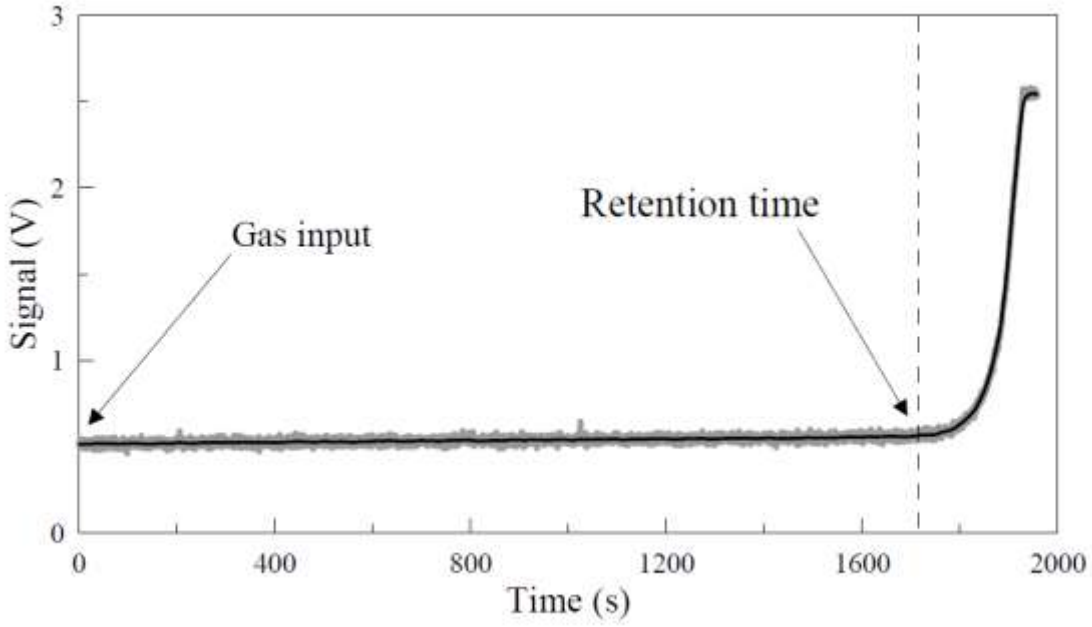

Figure 4. Time dependent evolution of the CO_2 or He concentration at the upper surface of the flux column. The gas standard enters from the base of the column since time zero. At the summit of the flux column, the target gas components have the baseline concentration until the inflated gas started to modify the concentration profile in the porous medium. The dashed line indicates the time when the CO_2 or He concentration at the top of the column starts to change. This time is considered as the retention time of the component (CO_2 or He) under the imposed laboratory conditions.

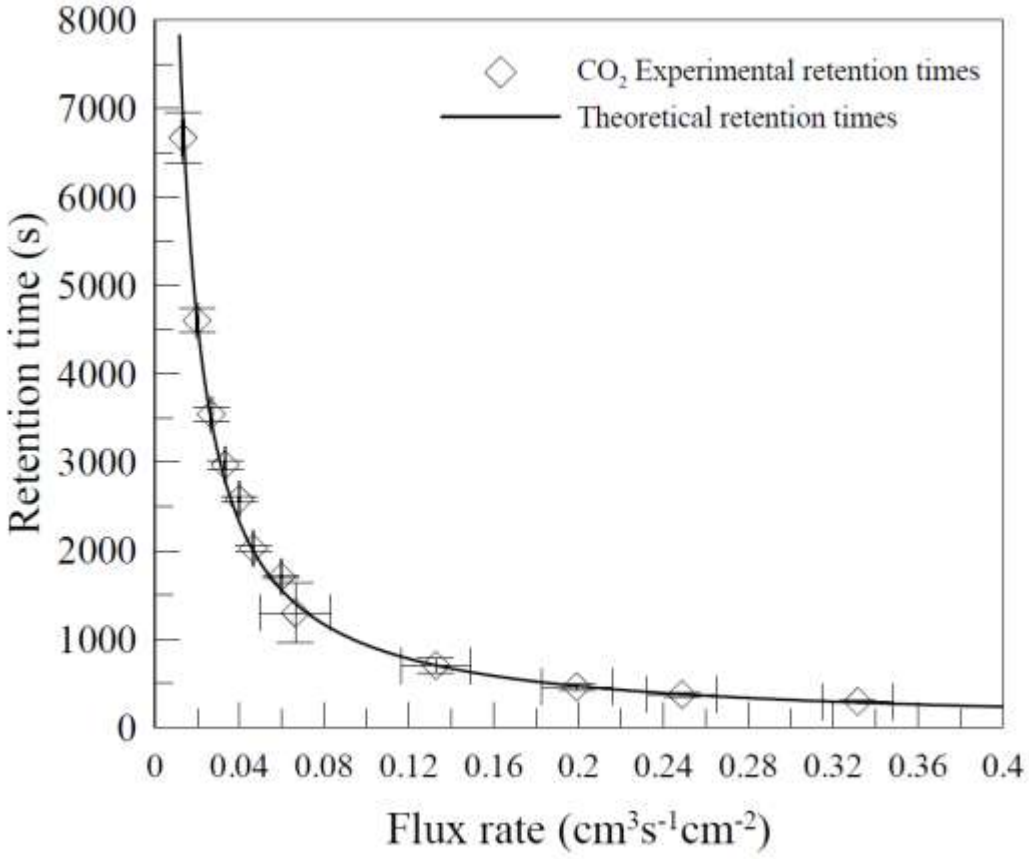

Figure 5. The experimental retention times of CO_2 as functions of the flux rate of the gas standard (CO_2 = 99.99 vol %). The flux rate (v) is expressed in $cm^3s^{-1}cm^{-2}$, and the retention times in seconds. The black line indicates the theoretical computation of the retention times as a function of the flux rate. The open diamonds are the experimental retention times of the CO_2 for fixed flux rates. The accuracy of the retention time was evaluated as a function of the accuracy of the measurement of the flux rate. The error bars are computed according to the accuracy of the measurement of the flux rate and the response time of the CO_2 sensor.

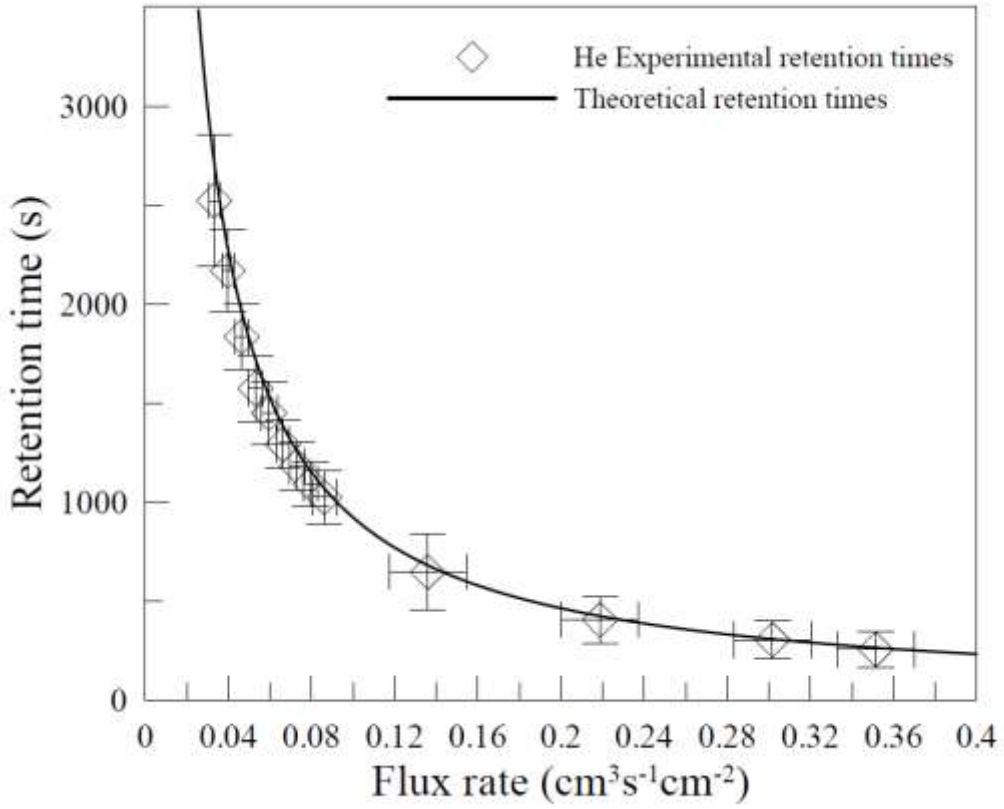

Figure 6. Retention times of He as a function of the flux rate of the gas standard. The flux rate is expressed in $cm^3s^{-1}cm^{-2}$, and the retention times in seconds. The black line indicates the theoretical computation of the retention times as a function of the flux rate. The open diamonds are the experimental retention times of the He for fixed flux rates. The accuracy of the retention time was computed as a function of the accuracy of the measurement of the flux rate. The error bars are computed according to the accuracy of the measurement of the flux rate and the response time of the He sensor.

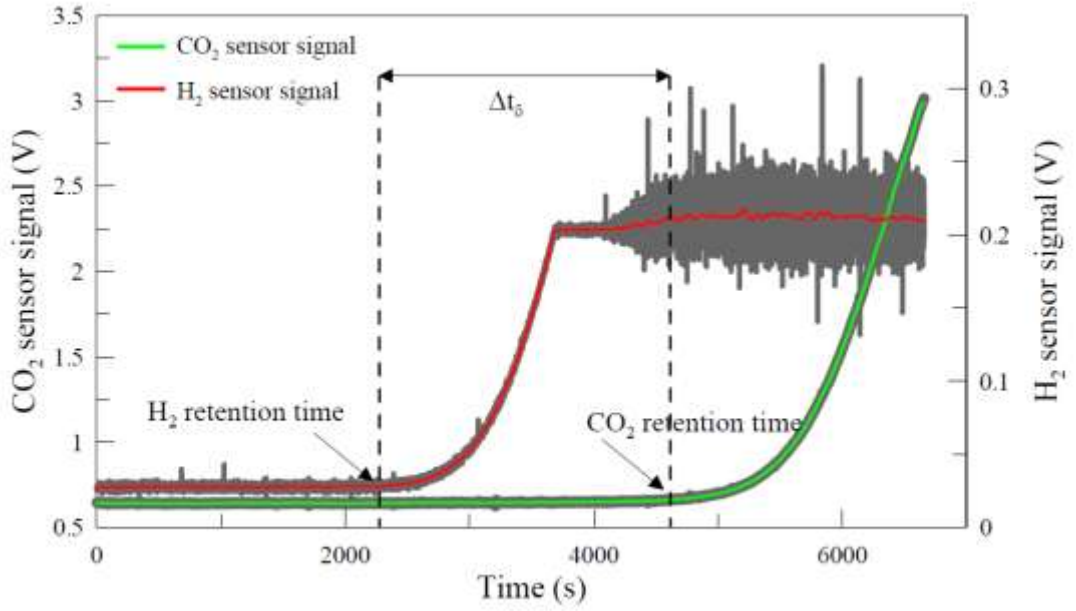

Figure 7. The time dependent evolution of both the H_2 and the CO_2 concentrations at the upper surface of the flux column using the MGM standard. The red line indicates the record of the H_2 sensor, and the green curve indicates the record of the CO_2 detector. The retention times of H_2 and CO_2 components are indicated with vertical black dashed lines. The difference in the retention times of the two components, referred to as the delay, is the result of a chromatographic effect in the porous medium.

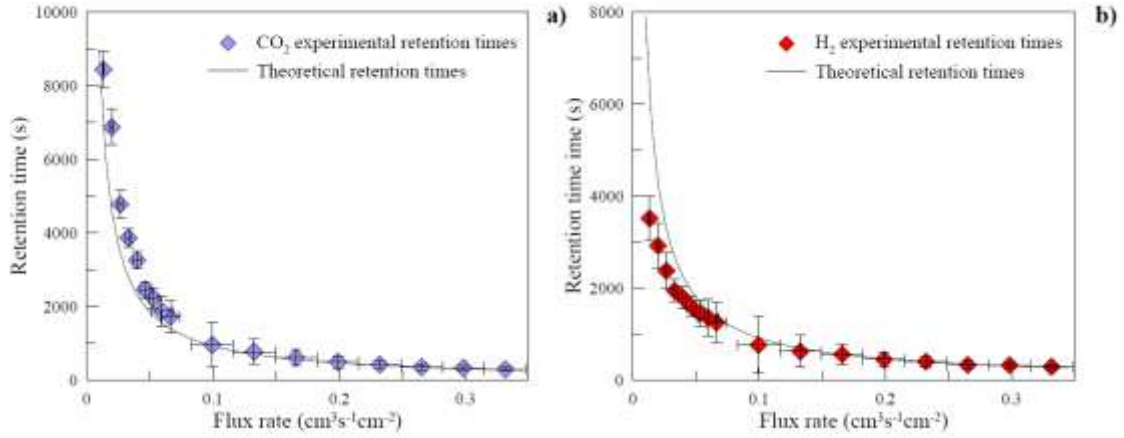

Figure 8. The experimental retention times of both CO_2, and H_2 as functions of the flux rate of the MGM standard. In Figure 8a, the black line is the theoretical curve of the retention times of CO_2 as a function of the flux rate, and the pastel blue diamonds indicate the experimental retention times measured by the tests. In Figure 8b, the black line is the theoretical curve of the retention times of H_2 as a function of the flux rate, and the red diamonds indicate the experimental retention times measured by the tests. The error bars are computed according to the accuracy of the measurement of the flux rate and the response time of the CO_2 and H_2 sensors.

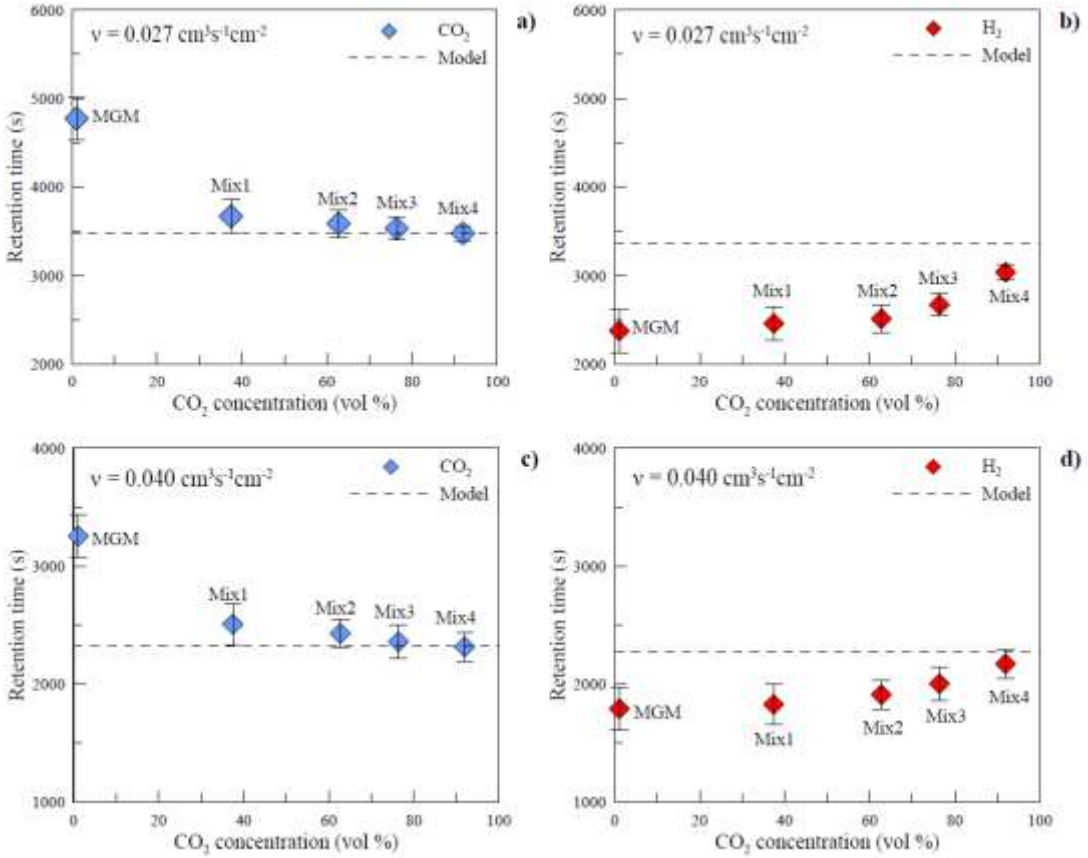

Figure 9. The compositional effect of the standard mixtures on the retention times of both CO_2, and H_2. The dashed lines indicate the theoretical retention times as a function of the flux rate of the gas standard. The retention times were measured with the MGM standard and the gas standards of intermediate composition between MGM and pure CO_2 (Mix1, Mix2, Mix3, and Mix4). The accuracy of the retention time was evaluated as a function of the accuracy of the measurement of the flux rate. Figure 9a collects the retention times of CO_2 measured at flux rate of 0.027 $cm^3s^{-1}cm^{-2}$; Figure 9b collects the retention times of H_2 measured at flux rate of 0.027 $cm^3s^{-1}cm^{-2}$; Figure 9c collects the retention times of CO_2 measured at flux rate of 0.040 $cm^3s^{-1}cm^{-2}$; Figure 9d collects the retention times of H_2 measured at flux rate of 0.040 $cm^3s^{-1}cm^{-2}$.

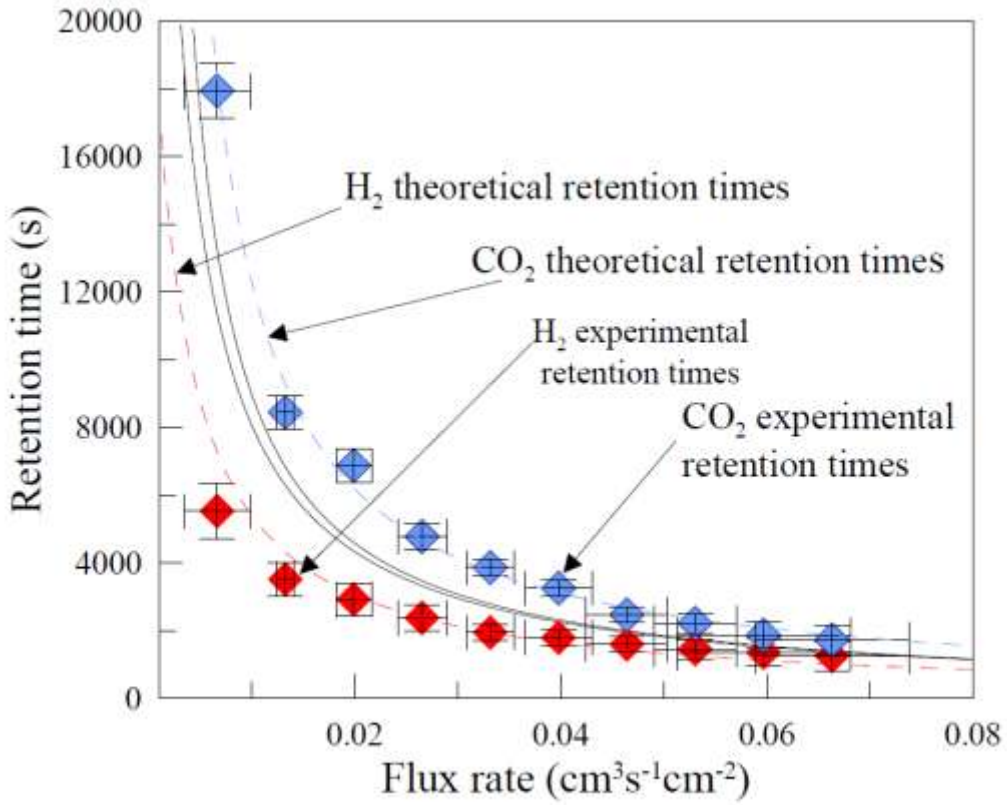

Figure 10 Retention times of CO_2 (a), and H_2 (b) measured at constant flux rate of $\nu = 0.006$ $cm^3s^{-1}cm^{-2}$ as function of the distance of the gas source from the detectors. c) Measured delays between CO_2 and H_2 as function of the distance between the gas source and the detectors.

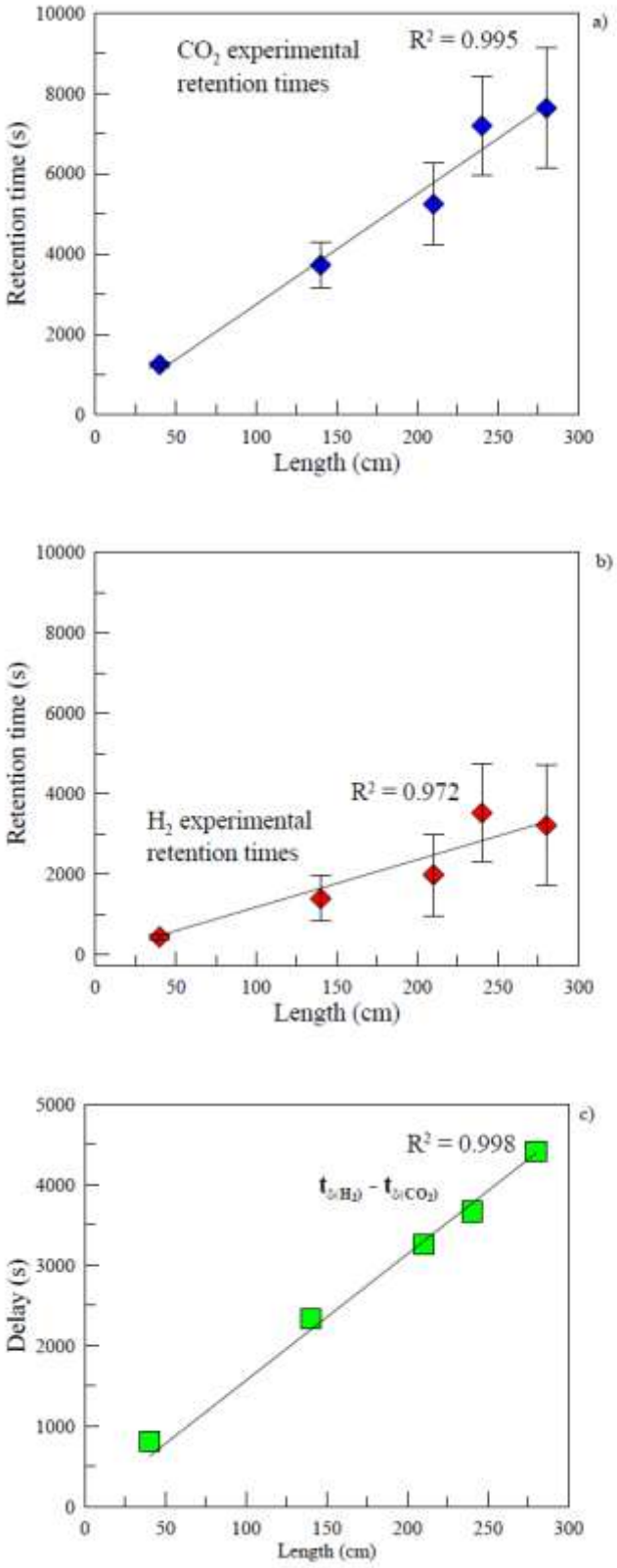

Figure 11 Retention times of CO_2 and H_2 in comparison to the model predictions. Black lines are the theoretical retention times computed with the binary diffusion coefficients of CO_2 and H_2 in air, respectively. Dashed lines are the theoretical computation with difference in the diffusivity of H_2 and CO_2 of 20% in comparison to the binary diffusivity.

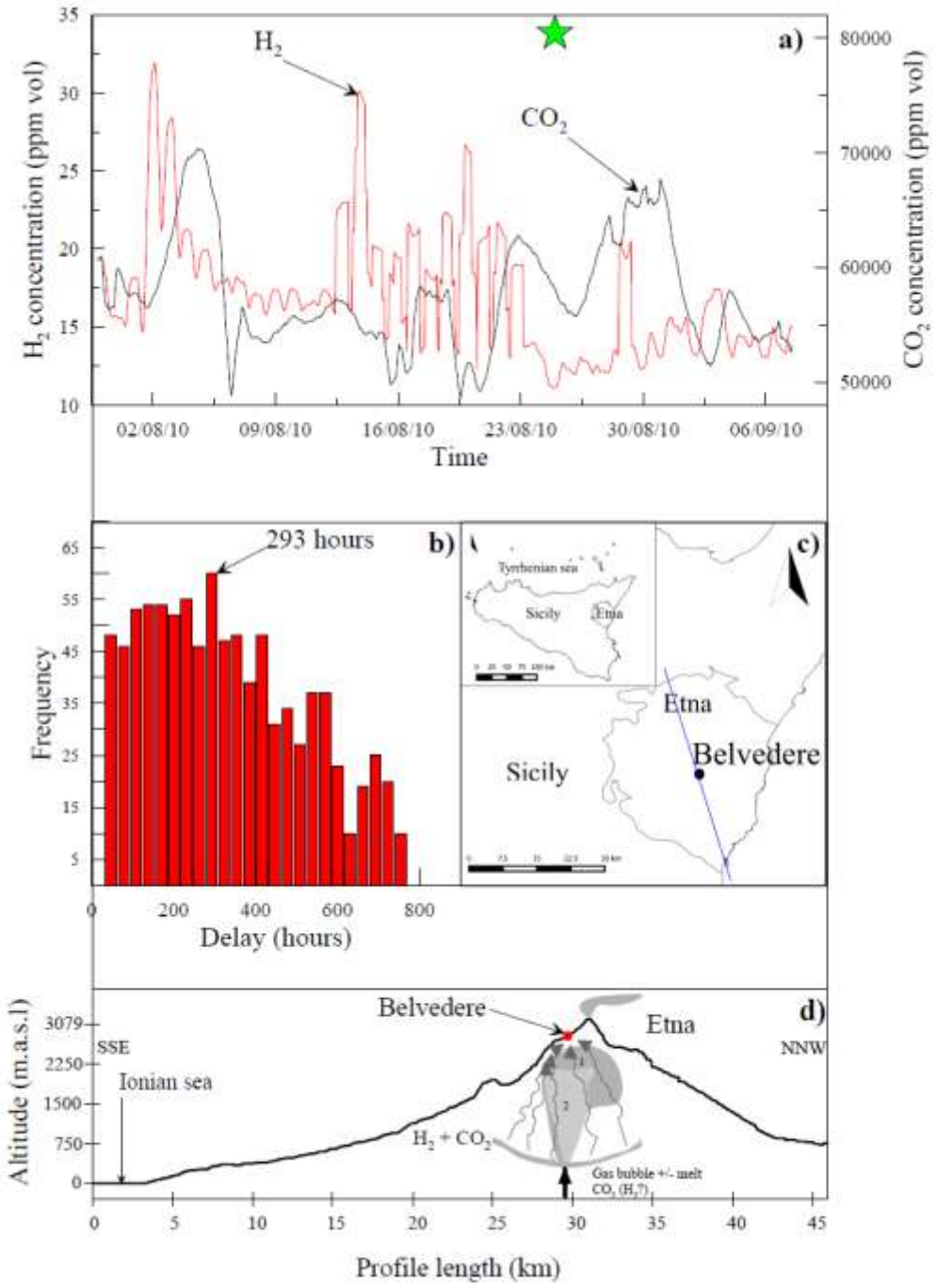

Figure 12 Continuous monitoring of H_2 and CO_2 at Etna volcano (data from *Di Martino et al.*, 2013). a) Time series of the average value of concentration of H_2 (red line) and CO_2 (black line); the values of the 17 hours moving average were attributed to the ninth hour. b) Frequency histogram of the delay of CO_2 and H_2 in the time window domain. c) Belvedere monitoring site. d) topographic profile of Etna volcano. The depths of the source of the volcanic tremor are reported (*Aiuppa et al.*, 2010b: **1**; *Andronico et al.*, 2013: **2**). The lower arc indicates the distance of the degassing source from where the H_2 and CO_2 start to move by advective-diffusive process calculated by the model reported in this paper. Green star indicates the explosive events occurred at Bocca Nuova Crater in August 25, 2010

Table 1. Binary diffusion coefficient (D_i^{th}–air) for CO_2, H_2 and He computed at different temperature and pressure according to the model of molecular diffusivity (Chapman and Cowling, 1970)

Component	**P = 0.1 MPa**				**P = 1 MPa**			
	293 k	**573 k**	**773 k**	**1273 k**	**293 k**	**573 k**	**773 k**	**1273 k**
$\mathbf{D_{CO_2\text{-}air}}$	0.16	0.51	0.87	2.08	0.01	0.05	0.09	0.21
$\mathbf{D_{H_2\text{-}air}}$	0.67	2.38	4.01	9.62	0.07	0.24	0.40	0.96
$\mathbf{D_{He\text{-}air}}$	0.58	2.24	3.78	9.06	0.06	0.22	0.38	0.91

Table 2. Chemical composition of the multicomponent mixtures used in the laboratory experiments. The chemical compositions of the mixtures were measured in the laboratory by chromatographic analysis with the Perkin Elmer Clarus 500 having Shincarbon ST 100/120 Mesh 3m x 1/8" OD column.

Name	He (ppm vol)	H_2 (ppm vol)	O_2 (vol %)	N_2 (vol %)	CO (ppm vol)	CH_4 (ppm vol)	CO_2 (vol %)
MGM standard	462.7	909.2	20.5	78.07	919.9	964.5	1.1
Mix1	245	413	12.35	50.50	411	429	37.42
Mix2	194	317	7.46	29.91	334	352	62.72
Mix3	117	190	4.50	17.92	205	215	76.37
Mix4	64	134	0.19	8.09	146	162	91.94

Table 3. Gas sensors and the target gas components used for performing the laboratory test.

Target gas species	Sensor	Response time
CO_2	Gascard II – range 0 - 1 vol %	10 s
H_2	City Technology H_2 sensor – range 0 - 2000 vol ppm	20 s
He	Alcatel ASM 100 HDS	1 s

Table 4. Theoretical retention times (t_{model}) of the CO_2 and experimental results ($t_{measure}$) measured in the laboratory with pure CO_2 in the flux simulator (CO_2 = 99.99 vol %). The RT CO_2 difference are computed as $100 \cdot (t_{measure} - t_{model})/t_{model}$. Negative values indicates that experimental RTs are shorter than theoretical computation.

Flux rate (v) ($cm^3\ s^{-1}\ cm^{-2}$)	**t_{model} (s)**	**$t_{measure}$ (s)**	**RT CO_2 difference (%)**
0.013	6877	6886	0.1
0.020	4620	4602	-0.4
0.027	3478	3465	-0.4
0.033	2789	2785	-0.1
0.040	2328	2301	-1.2
0.046	1997	2022	1.3
0.060	1556	1564	0.5
0.066	1412	1310	-7.2
0.133	709	705	-0.6
0.199	474	461	-2.7
0.249	381	377	-1.0
0.332	281	290	3.2

Table 5. Theoretical retention times (t_{model}) and experimental results ($t_{measure}$) obtained with pure He in the flux simulator. The RT He difference are computed as $100 \cdot (t_{measure} - t_{model})/t_{model}$. Negative values indicates that experimental RTs are shorter than theoretical computation.

Flux rate ($cm^3\ s^{-1}\ cm^{-2}$)	t_{model} **(s)**	$t_{measure}$ **(s)**	**RT He difference (%)**
0.033	2723	2522	-7.4
0.039	2281	2167	-5.0
0.046	1963	1834	-6.6
0.053	1723	1573	-8.7
0.059	1535	1449	-5.6
0.066	1384	1292	-6.6
0.073	1260	1181	-6.3
0.080	1156	1091	-5.6
0.086	1068	1024	-4.1
0.135	680	646	-4.9
0.218	424	405	-4.4
0.302	308	304	-1.1
0.351	264	256	-3.0

Table 6. Theoretical retention times and experimental data for both the CO_2 and the H_2 measured in the laboratory with the MGM standard. Both the RT CO_2 difference and RT H_2 difference are computed as $100 \cdot (t_{measure} - t_{model})/t_{model}$. Negative values indicates that experimental RTs are shorter than theoretical computation.

Flux rate ($cm^3\ s^{-1}\ cm^{-2}$)	$CO_2\ t_{model}$ (s)	$CO_2\ t_{measure}$ (s)	RT CO_2 difference (%)	$H_2 t_{model}$ (s)	$H_2\ t_{measure}$ (s)	RT H_2 difference (%)
0.007	13449	17933	33.3	11904	5526	-53.6
0.013	6877	8438	22.7	6449	3514	-45.5
0.020	4620	6872	48.7	4423	2920	-34.0
0.027	3478	4774	37.3	3365	2375	-29.4
0.033	2789	3862	38.5	2716	1943	-28.5
0.040	2328	3254	39.8	2277	1792	-21.3
0.046	1997	2465	23.4	1960	1595	-18.6
0.053	1749	2215	26.6	1720	1455	-15.4
0.060	1556	1867	20.0	1533	1354	-11.7
0.066	1401	1726	23.2	1382	1249	-9.6
0.099	935	955	2.1	927	764	-17.6
0.133	702	774	10.3	697	623	-10.6
0.166	562	610	8.5	559	557	-0.4
0.199	468	493	5.3	466	447	-4.1
0.232	402	423	5.2	400	401	0.3
0.265	351	353	0.6	350	328	-6.3
0.298	312	330	5.8	312	324	3.8
0.332	281	295	5.0	280	290	3.6